Available online at www.sciencedirect.com
ScienceDirect
Ceramics International 38 (2012) 895–900
CERAMICS INTERNATIONAL
www.elsevier.com/locate/ceramint

Synthesis and characterization of $B_{13}C_2$ boron carbide ceramic by pulsed electric current sintering

Song Zhang [a,*], Wenzhong Lu [a], Chuanbin Wang [b], Qiang Shen [b], Lianmeng Zhang [b]

[a] Department of Electronic Science and Technology, Huazhong University of Science and Technology, 1037 Louyu Road, Wuhan 430074, People's Republic of China
[b] State Key Laboratory of Advanced Technology for Materials Synthesis and Processing, Wuhan University of Technology, Wuhan 430070, People's Republic of China

Received 25 April 2011; received in revised form 9 May 2011; accepted 9 May 2011
Available online 13 May 2011

Abstract

Approximately 400 nm grain sized boron–carbon ceramic was synthesized by the pulsed electric current sintering (PECS) method using boron and carbon powders. Relative density of up to 95% was achieved at sintering temperature of 1900 °C. This ceramic was composed with $B_{13}C_2$ as major phase and few B_4C and C, which were characterized by X-ray diffraction (XRD) and Rietveld refinement quantitative analysis and chemical analysis (CA) and electron probe microanalysis (EPMA). The microstructure was also observed via transmission electron microscope (TEM).

Keywords: $B_{13}C_2$; B_4C; Pulsed electric current sintering (PECS); Phase; Microstructure

1. Introduction

Boron carbide (B_4C) is the third hardest material next to diamond and cubic boron nitride (CBN) [1], and it is the hardest material above 1300 °C [2]. Combined with low density and high Young's modulus, it is attractive for application in lightweight armor and wear-resistant parts [3,4]. Boron carbides reported high chemical stability and oxidation resistance [5], and thus it has been researched as a high-temperature semiconductor or thermoelectric material [6,7]. B_4C is also widely used as a neutron-absorbing control rod material [8]. In recent years, boron carbide has played a very important role in fusion nuclear reactor inner wall [9,10].

However, because of the rigid covalent bond and corresponding low diffusion mobility, the sintering of the pure boron carbide is very difficult. Without additives, dense boron carbide can only be obtained at temperatures above 2200 °C by hot pressing or pressureless sintering [11,12]. Direct synthesis of the boron carbide ceramic from B and C elements with B/C molar ratio of 4.0:1 had been researched by hot pressing (HP) [13] and pulsed electric current sintering (PECS) [14] methods, which effectively lowered the sintering temperature. The sintered materials had been thought to be $B_{4.0}C$ without enough proof, and there were graphite diffraction peaks defected from the XRD patterns. The patterns of B_4C (PDF2 35-0798) and $B_{13}C_2$ (PDF2 71-0099) are very similar and the phase of sintered boron carbide in the past reports could not be identified actually only depend on XRD results. In fact, boron carbide is a solid solution stable over the compositional range of 8–20 at.% C [15]. It is generally accepted that boron carbide has a complex rhombohedral structure in which $B_{11}C$ icosahedra are linked by a chain of C–B–C bonds along the main diagonal of the rhombohedron. With increasing boron content, C–B–C chains are replaced by C–B–B [11]. Boron carbide (B_xC_y) of other stoichiometries have potential applications, especially in the nuclear industry [16] and for their thermoelectric properties [11].

In the present study, a kind of boron-rich boron carbide ceramic was prepared by the PECS method, in which the material was in situ synthesized from carbon and boron powders and densified simultaneously by a pulsed electric current sintering (PECS) technique. The phase and microstructure of the material were mainly investigated.

* Corresponding author.
E-mail address: superkobe0104@hotmail.com (S. Zhang).

0272-8842/$36.00 © 2011 Published by Elsevier Ltd and Techna Group S.r.l.
doi:10.1016/j.ceramint.2011.05.036

2. Experimental procedure

The starting materials were boron and carbon powders (Goodfellow Cambridge Limited) with the particle size of less than 0.5 μm and 20–50 μm, respectively. The purity of the powders was up to 99.9%. They were mixed in molar ratios of 4.0:1.

The mixed powders were put into a graphite die with diameter of 32 mm and then sintered by a PECS furnace (Dr. Sinter 1050 SPS, Sumitomo Coal Mining Co., Tokyo, Japan). The sintering temperature was changed from 1300 to 1900 °C while the heating rate was 100 °C per minute and the pressure was fixed at 20 MPa. The PECS process was performed in vacuum (10^{-3} Pa) for 20 min with 3 min for holding time. During the whole sintering process, the displacement along the vertical axis of the push-rod was recorded.

The density of the prepared samples was measured via Archimedes' method. The crystalline phases were examined by powder X-ray diffractometer (XRD, Philips X'pert pro, θ-θ) with CuKα radiation (40 kV, 40 mA). The B/C molar ratio of sintered material was determined by chemical analysis method in a platinum crucible. Micro-area chemical analysis was employed by Electron Probe Microanalysis (EPMA, JXA8800R). Transmission electron microscopy (TEM; JEOL, JEM-2010, operated at 200 kV) was used to observe the microstructure.

The ''Rietveld method'' could create an effective separation of overlapping data, thereby allowing an accurate determination of the crystal structure by considering the practical diffraction factors, such as atomic scattering factors and thermal parameters. Rietveld's profile analysis method was employed for refinements using the Maud program. The X-ray diffraction pattern for the main phase was assigned to a rhombohedral structure. Time for acquiring refinement data was 30 h for the range of 20–90° 2θ, leading to good statistics, the step 0.02° (2θ) with a fixed counting time of 30 s, allowing excellent definition to reflection peaks.

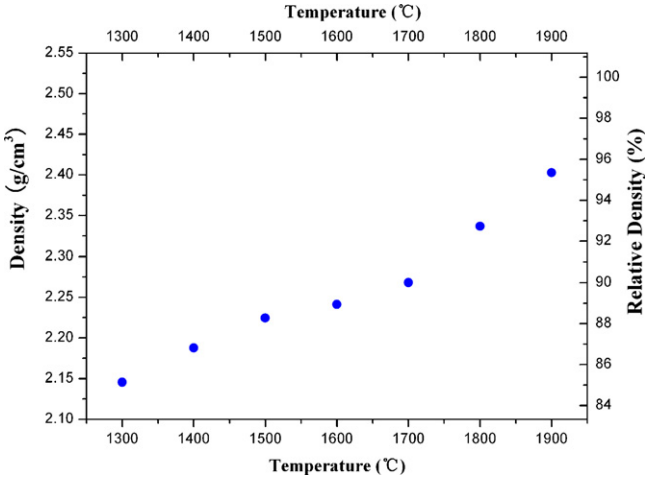

Fig. 1. Densities of specimens sintered at different temperature.

3. Results and discussion

3.1. Densification

The densities of the boron carbide samples sintered at 1300–1900 °C are shown in Fig. 1. The density of material increased with increasing sintering temperature and a relative density of over 95% was obtained at 1900 °C. Fig. 2 shows the displacement along the vertical axis of sample, which depicts the shrinking behavior during the 1900 °C sintering. It can be seen that two sharp steps in the shrinkage, marked as step 1 and step 2 were observed indicating two typical densification processes.

3.2. Phase

The XRD patterns of boron carbide sample sintered at a temperature range of 1300–1900 °C are shown in Fig. 3. From this figure, the intensity of graphite (0 0 2) peaks were fading

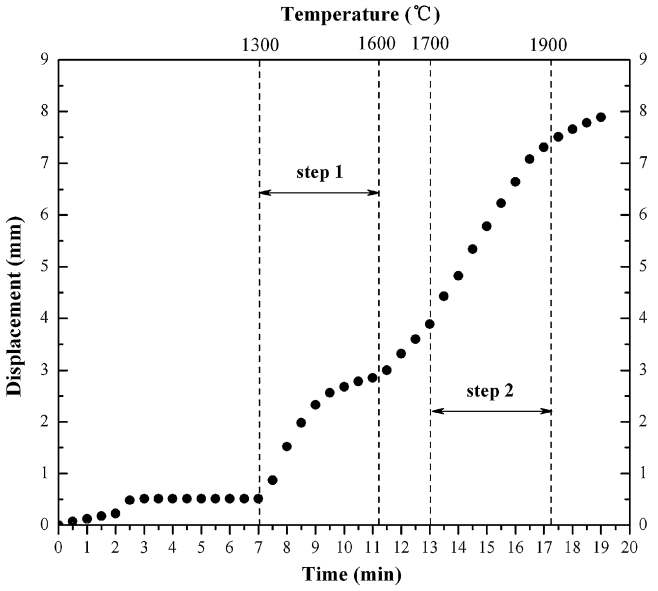

Fig. 2. Shrinking curve for boron carbide SPS sample.

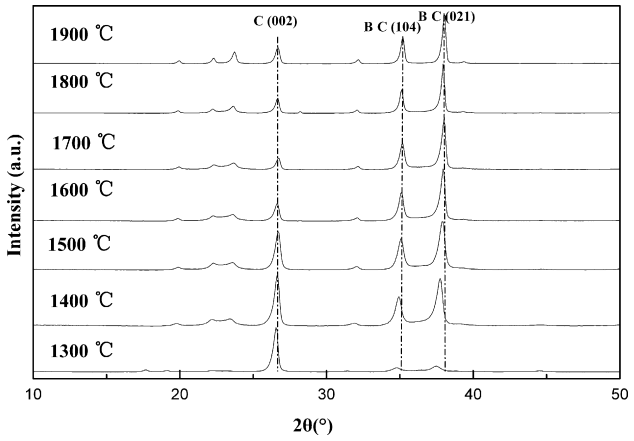

Fig. 3. X-ray diffraction patterns of boron carbide sintered by SPS at 1300–1900 °C.

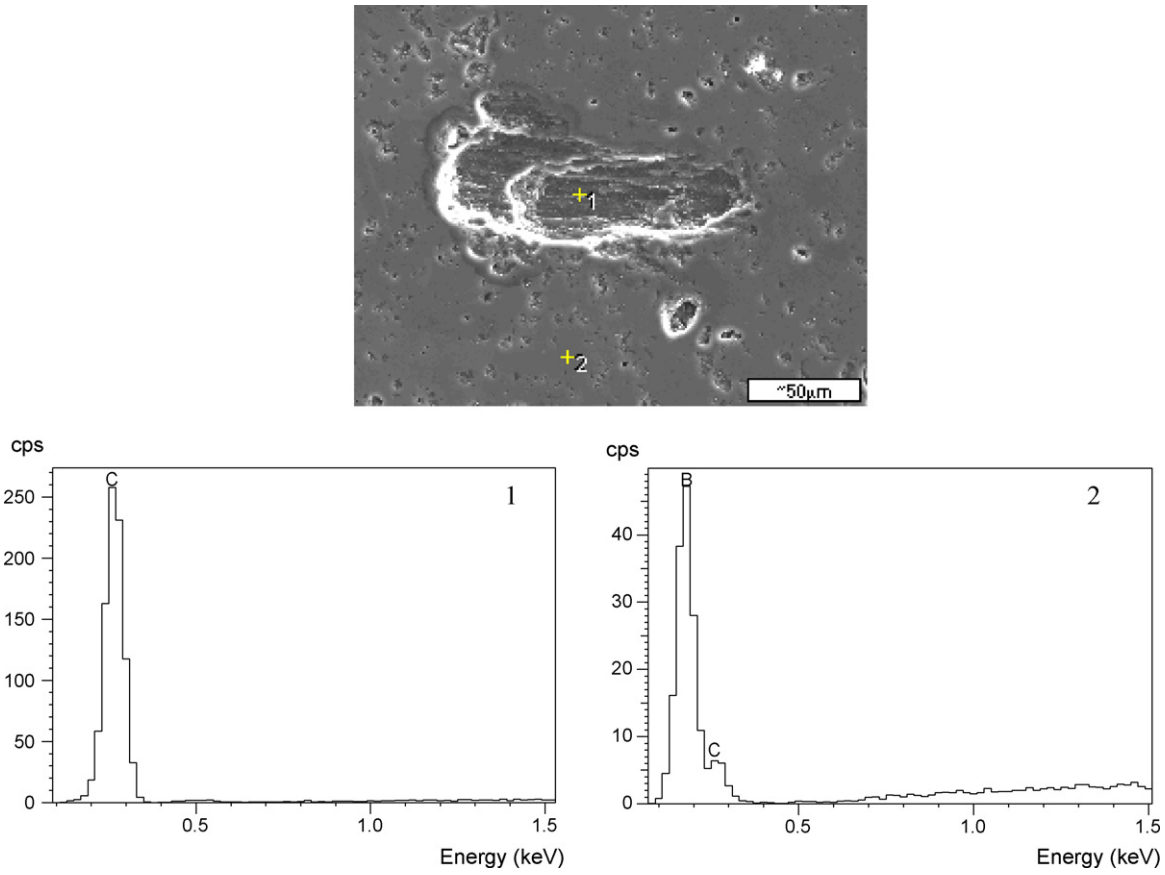

Fig. 4. The EPMA results of the boron carbide sintered by SPS at 1900 °C.

while the peaks of boron carbide (0 2 1) and (1 0 4) were shown with increasing temperature from 1300 °C to 1600 °C, which corresponded to the synthesis of boron carbide from boron and carbon powders. This reaction took place rapidly in 3 min, shown as step 1 in Fig. 2. At this stage, diffraction peak positions of boron carbide were shifting to higher Bragg angles with the increasing of sintering temperature, indicating the decrease of lattice parameters. To confirm the chemical composition, a chemical analysis method was employed for determining the B/C molar ratio of sintered (at 1900 °C) material, and the results showed the ratio did not change during the PECS process. On the other hand, the diffraction peaks of boron were not yet observed in the XRD patterns. Thus, the existence of free carbon indicates the main phase of sample was a kind of boron-rich carbide in step 1. As a result, the phases of the sintered samples were free-C and B-rich boron carbide ($B_{4+x}C$). When the temperature was increased, more C atoms ($r = 0.77$ Å) diffused into the $B_{4+x}C$ lattices and replaced B atoms which had a larger atom radius ($r = 0.82$ Å). As a result, the lattice parameters of boron carbide were reduced. Our

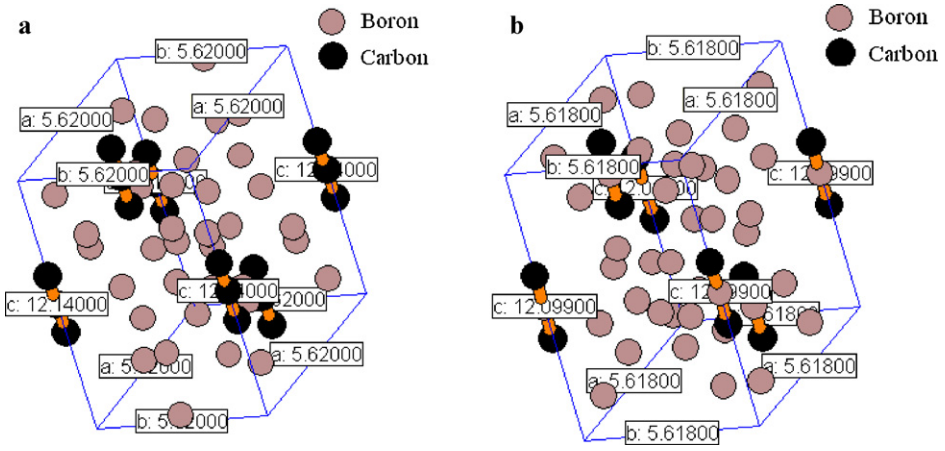

Fig. 5. Crystal structure of (a) B4C and (b) B13C2.

results were in accord with Frank's study [17]. In step 2 (1700–1900 °C), the shift of $B_{4+x}C$ (0 2 1) and (1 0 4) peaks were not observed, the intensity of those peaks was shown to be sharper and sharper which mean a growth of grains.

Free carbon was observed even at the sintering temperature reached 1900 °C (Fig. 3). The same phenomenon occurred in Heian's study [14], but he did not give any explanation. Though, in our work, we have taken the EPMA method for investigation of the free carbon which was in the sintered materials. The scanning results (Fig. 4) show the strong C peak on a rock-like grain ($^{+}$1) and B, C peaks on the other smooth area ($^{+}$2). The geometry of rock-like grain is very similar with the graphite element powder that indicates the free carbon is the remains of raw powder. Moreover, the B/C molar ratio obtained by EPMA is not accurate because of that B, C elements are over the measurement range of the EPMA. In addition, the B_4C (PDF2 35-0798) and $B_{13}C_2$ (PDF2 71-0099) have the similar crystal structure (Fig. 5) in the series of boron carbide which is mentioned in Section 1. The details of XRD patterns of sintered material at high Bragg angles (60–90°, because PDF2 35-0798 and 71-0099 are almost same at low angles) is shown as Fig. 6. Compared with the XRD patterns of synthesized boron carbide, $B_{13}C_2$ matched more exactly than B_4C in the regions of 65–68° and 78–85°. In order to further identify the phase structure and quantify each phase of obtained material, the Rietveld refinement was employed. The refinement of B_4C, $B_{13}C_2$ and C were done starting from Table 1, and the calculations were performed in the R−3m: H and P63/mmc space groups with Maud program. Fig. 7 and Table 2 show the refinement results and graphical representation of the final Rietveld refinement. A good match of the peak positions was achieved from the refinement including the lattice and background parameters, and then the peak profile and asymmetry parameters were refined. Residuals from the refinement were calculated to be 11.41% for R_{wp}, and 10.51 for R_{exp}, which means the refinement result is credible. From Table 2, volume fraction and weight fraction were obtained for B_4C, $B_{13}C_2$ and C, and then the results of refinement indicated that the ceramic was almost totally $B_{13}C_2$. Furthermore, Maud program calculated the grain size of material was 410 nm, which was in accord with TEM results mention in the next section.

Table 1
Initial parameters of each phase.

Phase	Space group	Cell detail	Atomic position
B_4C	R−3m:H	$a = b = 5.62$ Å $c = 12.14$ Å	B1(0.1667, −0.1667, 0.36) B2(0.106, −0.106, 0.113) C1(0, 0, 0. 5) C2(0, 0, 0.385)
$B_{13}C_2$	R−3m:H	$a = b = 5.61$ Å $c = 12.09$ Å	B1(0.1631, −0.1631, 0.6411) B2(0.2256, −0.2256, 0.7801) B3(0, 0, 0.5) C1(0, 0, 0.6175)
C	P63/mmc	$a = 2.47$ $c = 6.72$	C1(0, 0, 0.25) C2(0.333, 0.666, 0.25)

3.3. Microstructure

The microstructure of boron carbide sample sintered at 1900 °C is shown in Fig. 8. A texture composed of fine grains was observed. From the TEM bright field (BF) images (Fig. 8a), the grain size of boron carbide was hundreds of nanometers, which was much smaller (∼400 nm) than those obtained by HP process with grain size of ∼30 μm [13]. The TEM figures also show a high density of parallel bright–dark lines, which is proved to be twins or stacking faults in the previous studies [14,18,19]. On the basis of TEM observations, Mackinnon et al. [20] proposed that stacking faults resided only in (0 0 1) plane. In Umberto's research [19], he performed computer simulation using the DIFFax program and concluded that the planar faults (such as twins and stacking faults) lied in the (0 0 1) plane of the original rhombohedral structure of boron carbide. In this work, the angle between bright–dark lines and (1 0 1) plane is 60° (Fig. 8b). Whereas, the angle between (0 0 1) and (1 0 1) plane was 55.3° in boron carbide lattice that indicating those defined planar faults within our material do not lie on the (0 0 1) plane as reported previously. We have searched right plane which angled the (1 0 1) plane 60° from all the plane of boron carbide, and the plane must satisfy the relationship of the formula in the

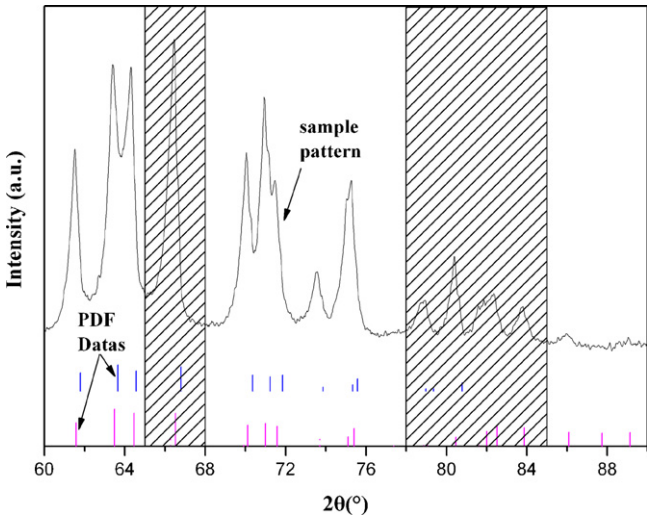

Fig. 6. Comparison between XRD pattern of synthesized sample and PDF cards of B4C (top) and B13C2 (bottom).

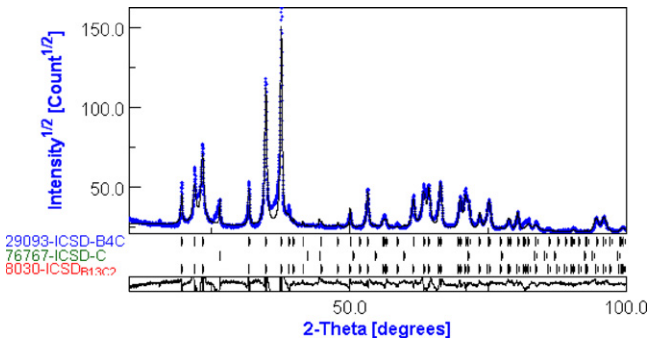

Fig. 7. Final Rietveld refinement results.

Table 2
Refinement results.

Phase	Space group	Cell detail	Atomic position	Volume fraction & weight fraction
B_4C	R−3m:H	$a = b = 5.62$ Å $c = 12.14$ Å	B1(0.1667, −0.1667, 0.36) B2(0.106, −0.106, 0.113) C1(0, 0, 0. 5) C2(0, 0, 0.385)	V: 1.85% W: 1.87%
$B_{13}C_2$	R−3m:H	$a = b = 5.63$ Å $c = 12.13$ Å	B1(0.16, −0.16, 0.644) B2(0.223, −0.223, 0.785) B3(0, 0, 0.5) C1(0, 0, 0.3823)	V: 97.59% W: 97.62%
C	P63/mmc	$a = 2.46$ $c = 6.71$	C1(0, 0, 0.25) C2(0.333, 0.666, 0.25)	V: 0.56% W: 0.51%

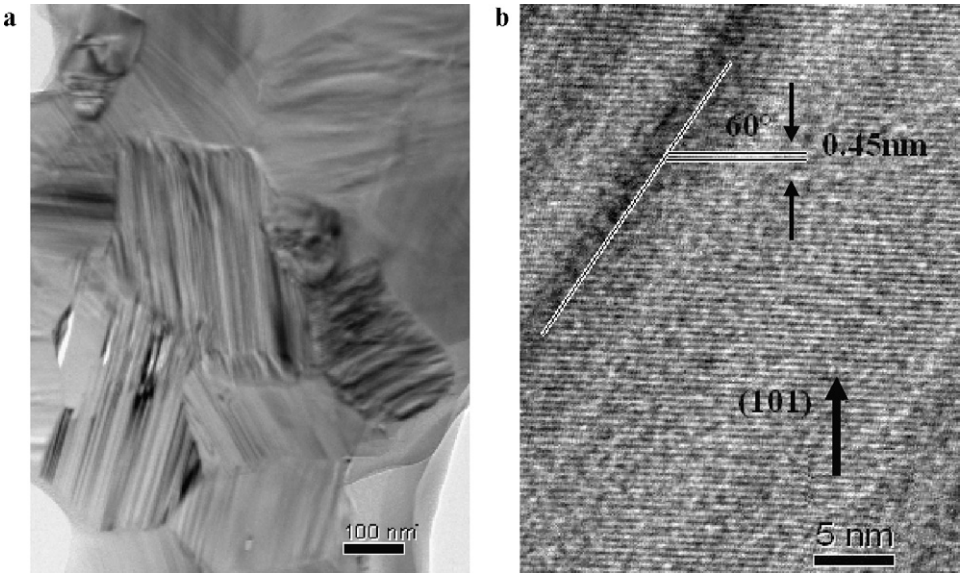

Fig. 8. TEM image for boron carbide sample; (a) bright-field image of nanometric structure and (b) high-resolution image of grain.

rhombohedral structure [21]:

$$\cos\phi = \frac{a^4 d_1 d_2}{V^2}[\sin^2\alpha(h_1h_2 + k_1k_2 + l_1l_2) + (\cos^2\alpha - \cos\alpha) \times (k_1l_2 + k_2l_1 + l_1h_2 + l_2h_1h_1k_2 + h_2k_1)$$

$\phi = 120^\circ$; $(h_1\ k_1\ l_1) = (1\ 0\ 1)$; $\alpha = 90^\circ$; $a = 5.618$ Å; $d_1 = 4.5$ Å in $B_{13}C_2$ rhombohedral R−3m (1 6 6) structure.

As a result, it shows the angle between (1 0 1) and (1 0 4) plane is 60°. In other words, those planar faults lay on (1 0 4) planes with small d value than (0 0 1) planes. Generally, the planar faults are likely to be within the planes, such as (0 0 1) planes, with large d value which caused by weak bond energy between them. This discrepancy between our work and the former may be caused by two factors: (1) The random distribution of carbon atoms on icosahedral site and substitution of C for B in the C–B–C chain in the $B_{13}C_2$ structure which cause carbon atoms bonded with weaker Van der Waal force in (1 0 4) planes. (2) Those bright–dark lines are not planar faults but the amorphous region [22] which is caused by the rapid PECS process. In addition, due to the low formation energies, stacking faults are very common with carbides. The pioneering work by Vijay and Cawley [23–25] showed that the presence of stacking faults, specifically twining, in hexagonal close-packed (*hcp*) structure caused broadening and shifing of certain peaks in XRD data relative to that expected from a material without such faults. And Paterson [26] did the same research in face-centered cubic (*fcc*) structure. At the same time, there is no difference in our XRD patterns between patterns without stacking faults.

4. Conclusions

A novel boron-rich boron carbide ceramic was prepared by carbon and boron powders and pulsed electric current sintering technology. It was found that the sintering process is made up of two steps, the reaction of boron and carbon powders and then the sintering of the material. The major phase is a kind of boron-rich boron carbide ($B_{13}C_2$), which was characterized by Rietveld refinement. The sample has a fine-microstructure, and a great amount of bright–dark lines had been observed in (1 0 4)

planes which might be caused by both the planar faults and amorphous regions.

Acknowledgement

This research was sponsored by National Natural Science Foundation of China, No.51102101.

References

[1] K.W. Lee, S.J. Harris, Boron carbide films grown from microwave plasma chemical vapor deposition, Diamond Related Materials 7 (10) (1998) 1539–1543.
[2] F. Thevenot, Boron carbide—a comprehensive review, Journal of the European Ceramic Society 6 (4) (1990) 205–225.
[3] J. Sun, H. Ling, Chemical structure and micro-mechanical properties of ultra-thin films of boron carbide prepared by pulsed-laser deposition, Tribology Letters 99–104 (July) (2004).
[4] Z.H. Han, G.Y. Li, Microstructure and mechanical properties of boron carbide thin films, Materials Letter 57 (4) (2002) 899–903.
[5] H.Y. Chen, J. Wang, H. Yang, W.Z. Li, H.D. Li, Synthesis of boron carbide films by ion beam sputtering, Surface and Coating Technology 128 (1) (2000) 329–333.
[6] T. Goto, J.H. Li, T. Hirai, Microstructure and thermoelectric properties of B–C–Y system composites, Transactions of the Materials Research Society of Japan 25 (1) (2000) 213–216.
[7] J.H. Li, T. Goto, T. Hirai, Thermoelectric properties of B_4C–SiB_n ($n = 4$, 6, 14) in-situ composites, Materials Transactions JIM 40 (4) (1999) 314–319.
[8] O. Gebhardt, D. Gavillet, SIMS imaging analyses of in-reactor irradiated boron carbide control rod samples, Journal of Nuclear Materials 279 (2-3) (2000) 368–371.
[9] I. Jiménez, D.G.J. Sutherland, T. van Buuren, J.A. Carlisle, L.J. Terminello, Photoemission and X-ray-absorption study of boron carbide and its surface thermal stability, Physical Review B 57 (20) (1998), 13167–13174.
[10] S. Vepřek, Large-area boron carbide protective coatings for controlled thermonuclear research prepared by in situ plasma CVD, Plasma Chemistry and Plasma Processing 12 (3) (1992) 219–235.
[11] M. Bouchacourt, F. Thevenot, The correlation between the thermoelectric properties and stoichiometry in the boron carbide phase B_4C–$B_{10.5}C$, Journal of Materials Science 20 (4) (1985) 1237–1247.
[12] N. Cho, Z. Bao, R. Speyer, Density- and hardness-optimized pressureless sintered and post-hot isostatic pressed B_4C, Journal of Materials Research 20 (8) (2005) 2110–2116.
[13] G.I. Kalandadze, S.O. Shalamberidze, A.B. Perkrishvili, Sintering of boron and boron carbide, Journal of Solid State Chemistry 154 (1) (2000) 194–198.
[14] E.M. Heian, S.K. Khalsa, J.W. Lee, Z.A. Munir, Synthesis of dense, high-defect-concentration B_4C through mechanical activation and field-assisted combustion, Journal of the American Ceramic Society 87 (5) (2004) 779–783.
[15] F. Thevenot, A review on boron carbide, Key Engineering Materials 57–68 (1991) 59–88.
[16] D.R. Tallant, T.L. Aselage, A.N. Campbell, D. Emin, Boron carbide structure by Raman spectroscopy, Physical Review B B40 (8) (1989) 5649–5656.
[17] F.W. Glaser, D. Moskowitz, An investigation of boron carbide, Journal of Applied Physics 24 (6) (1953) 731–734.
[18] K.H.G. Ashbee, Defects in boron carbide before and after neutron irradiation, Acta Metallurgica 19 (10) (1971) 1079–1085.
[19] A.-T. Umberto, M. Ohyanagi, Z.A. Munir, Modeling studies of the effect of twins on the X-ray diffraction patterns of boron carbide, Chemistry of Materials 16 (22) (2004) 4347–4351.
[20] I.D.R. Mackinnon, T.L.S. Aselage, B. Van Deusen, High resolution imaging of boron carbide nanostructures, American Institute of Physics Conference Proceedings 140 (1986) 114–118.
[21] Rigaku, X-ray Diffraction Handbook, Appendix 44, 1987.
[22] M. Chen, J.W. McCauley, K.J. Hemker, Shock-induced localized amorphization in boron carbide, Science 299 (2003) 1563–1566.
[23] V.V. Pujar, J.D. Cawley, Microstructure/properties relations of advanced materials computer simulations of diffraction effects due to stacking faults in-SiC. I. Simulation results, Journal of the American Ceramic Society 80 (7) (1997) 1653–1662.
[24] V.V. Pujar, J.D. Cawley, Computer simulations of diffraction effects due to stacking faults in β-SiC. II, Journal of the American Ceramic Society 84 (11) (2001) 2645–2651.
[25] V.V. Pujar, J.D. Cawley, Effect of stacking faults on the X-ray diffraction profiles of β-SiC powders, Journal of the American Ceramic Society 78 (3) (1995) 774–782.
[26] M.S. Paterson, X-ray diffraction by face-centered cubic crystals with deformation faults, Journal of Applied Physics 23 (8) (1952) 805–811.